VVS2019-5124

EXPLORING THE UNCERTAINTY IN THE EQUATION OF STATE FOR A HIGH EXPLOSIVE FIT TO HETEROGENEOUS DATA

Stephen A. Andrews
XCP-8 Verification and Analysis
Los Alamos National Laboratory
Los Alamos, NM 87547
Email: saandrews@lanl.gov

Andrew M. Fraser
XCP-8 Verification and Analysis
Los Alamos National Laboratory
Los Alamos, NM 87547
Email: afraser@lanl.gov

Scott I. Jackson
M-9 Shock and Detonation Physics
Los Alamos National Laboratory
Los Alamos, NM 87547
Email: eanderson@lanl.gov

Eric K. Anderson
M-9 Shock and Detonation Physics
Los Alamos National Laboratory
Los Alamos, NM 87547
Email: sjackson@lanl.gov

ABSTRACT

The extreme pressures and temperatures of the gas produced by detonating a High Explosive (HE) make it difficult to use experimental measurements to estimate the Equation Of State (EOS), the physics model that relates pressure, temperature, and density of the gas. Instead of measuring pressure directly one measures effects like the acceleration of metals driven by the HE. Typically one fits a few free parameters in a fixed functional form to measurements from a single experiment. The present work uses the optimization tool F_UNCLE to incorporate data from multiple experiments into a single EOS model for the gas produced by detonating the explosive PBX 9501. The model is verified by comparison to an experiment from outside the set of calibration data. The uncertainty in the EOS is also is examined to determine how each calibration experiment constrains the model and how the uncertainty arising from all calibration experiments affects predictions. This work identifies an EOS for HE detonation products and uncertainty about the EOS.

Nomenclature
Symbols

α_m	Magnitude of uncertainty in the isentrope
η	Deviation from the model degrees of freedom
Γ	Grüneisen gamma
ρ	Density
ρ_o	Material density at initial state
σ_m	Characteristic distance of correlation in uncertainty of the isentrope
θ	Model degrees of freedom
θ_μ	Prior model degrees of freedom
$\Upsilon(\rho)$	Optimization basis of orho-normal eigenfunctions

Variables

$B(\rho)$	The cubic B-spline basis function matrix
$b(\rho)$	B-spline basis function
C	Intercept of linear Us - U_p model
c_i	B-spline basis function coefficient
e	Mass-specific internal energy
P	Probability density function
$p_s(\rho)$	The function representing pressure as a function of density on the CJ isentrope
s	Slope of linear U_s - U_p model
U_p	particle speed
U_s	Shock speed

$\mathscr{Y}$ The set of data from all experiments
Modifiers
β_s Property of β on an isentrope
$\beta^\star$ Optimal value of β

1 Introduction

Mathematical models of physical processes are needed for computer simulations of complex systems. Current practice is to select a mathematical form with some small set of adjustable parameters and, typically, use a single experiment to calibrate the parameter set. Such an approach is common when determining Equation of State (EOS) models for High Explosive (HE) detonation products. A very popular approach for modeling an HE EOS is the JWL model [21] which is composed of two exponential terms and one power law term and has six free parameters. These six free parameters are fit to match the observed detonation velocity, pressure and energy as well as the velocity history observed in a cylinder experiment [10], discussed subsequently in Section 4.1. JWL models calibrated in this way have been shown to perform well when examining cylinder tests but have challenges predicting experiments which occur at regimes in density which was not reached in the cylinder test.

Alternatives to the JWL model have been proposed by Davis [3] (7 degrees of freedom), Hixson [15] (13 degrees of freedom) and Menikoff [24] (25 degrees of freedom). These models are also restricted to a fixed functional form. A semi-parametric approach represents the function as a weighted sum of continuous basis-functions. In the limit of an infinite number of basis functions, any function can be represented. In practice when a large (≈ 75) number of basis functions are used, there exists a function within the span of this basis which is 'close' to most functions. This semi-parametric approach means that the initial ideas of how the function should look do not constrain the possible model forms.

The semi-parametric approach still requires some procedure to calibrate the basis function coefficients to match experimental data. Optimization with a Bayesian objective function has been shown to have many advantages [1]. The objective function in the optimization is the log-posterior probability which is the sum of the log-prior probability, reflecting the prior state of knowledge about what the model should be, and the log-likelihood, reflecting what model is suggested by the data. Computing the likelihood of multiple experiments given a model provides a valid basis to compare the effects of a model on many different experiments. The total log-likelihood of all the experiments is simply the sum of each experiment. The relative importance of each experiment is given by the uncertainty in the experimental data rather than by some arbitrary weighting factor. It is important to note that not all experiments are suitable for use in such an optimization. It is assumed that there is no systemic bias in the experiments and that there should exist one model which can represent all experiments. Experiments in the 'unit-tier validation problem' category of Oberkampf and Roy [26] are good candidates for this optimization procedure since they are designed to be simple, with a small set of interacting physics processes and well characterized geometry and initial conditions.

Another advantage of using a Bayesian objective function is that the optimization of the basis function coefficients can be reduced to a simple quadratic problem which is easy to solve. The procedure requires very few evaluations of the objective function to obtain a solution, so expensive computer simulations can be used directly in the optimization problem rather than relying on a surrogate model. Finally, using a probabilistic objective function provides some insight into the uncertainty in the optimization results.

Overall, the approach described in this paper has four important advantages over previous efforts. First, by using multiple experiments, the model can be calibrated over a wider regime in density than any single experiment could consider. Second, the efficient formulation of the optimization problem allows expensive computer simulations that include all the relevant physics processes needed to accurately model a real experiment. Third, by using a semi-parametric formulation, a much wider range of possible functional forms can be considered. Finally, the predictive ability of the model to be assessed by exploiting the Bayesian formulation to produce both a mean function and functions bounding the uncertainty in the model.

Section 2 describes the optimization methods and Section 3 describes the uncertainty quantification methods. The experiments used to calibrate the model are described in 4. The results of the optimization as well as a validation and uncertainty quantification study are given in Section 5. Conclusions are given in Section 6.

2 Optimization Methods

The EOS for the HE detonation products is modeled using a Mie Grüeneisen approach,

$$p(\rho, e) = p_s(\rho) + \rho \Gamma(\rho)(e - e_s(\rho)). \tag{1}$$

In general, two functions are needed for this EOS, a function for the reference curve $p_s(\rho)$ and for the Grüeneisen gamma, $\Gamma(\rho)$. In this work, only the reference curve is treated as variable. The Grüeneisen gamma function is not optimized and is set to be:

$$\Gamma(\rho) = 0.6218. \tag{2}$$

2

The reference curve is the isentrope passing through the Chapman-Jouguet state, *i. e.* the state at which a detonation is self-supporting. This isentrope is a convenient reference curve as the energy along the curve is a simple integral involving pressure function.

The HE EOS model also required a nominal density of the reactants in order to compute properties at the CJ state. The reactants density was considered to be a property of the EOS and was fixed to the nominal density of PBX 9501, $1.835 \, \text{g cm}^{-3}$.

2.1 Representing the isentrope

The optimization seeks some function to represent the isentrope passing through the CJ point for the material. This continuous function is represented as the weighted sum of a set of cubic B-spline basis functions. See [9] for more details on how these basis functions are formulated and their properties.

$$p(\rho) = \underbrace{\begin{bmatrix} b_1(\rho) \ b_2(\rho) \ \ldots \ b_n(\rho) \end{bmatrix}}_{\text{B}(\rho)} \cdot \underbrace{\begin{bmatrix} c_1 \\ c_2 \\ \ldots \\ c_n \end{bmatrix}}_{c} \quad (3)$$

By using a large number of basis functions, a wide range of possible functions can be considered, with the consequence that some may be physically implausible; Section 2.2 discusses how the optimization procedure deals with this challenge.

The coefficients, c_i of the B-spline basis are one possible set of coordinates in which to perform the optimization. In this work, however, a different set of coordinates are used, the coefficients of an ortho-normal set of eigenfunctions of a kernel function expressed in the B-spline basis. This new basis has advantages when interpreting the results and also prevents numerical instability in the optimization. More details on why this basis was chosen, how it was created and its advantages in the optimization problem are given in [1].

The kernel function is of a 'squared exponential' form [31] which has two free hyper-parameters. One parameter, α_m, describes the uncertainty in the pressure on the isentrope across all densities. The other parameter σ_m describes the characteristic distance, in log-density, across which the uncertainty in pressure is correlated. Additional details are given in [1]

The final expression for the isentrope functions is:

$$p(\rho) = \Upsilon(\rho) \left(\theta + \theta_\mu \right), \quad (4)$$

where $\Upsilon(\rho)$ is the basis of ortho-normal eigenfunctions, θ are the model degrees of freedom and θ_μ is a vector of constants

representing a 'prior' function. In the process of constructing the basis $\Upsilon(\rho)$, the model was constructed as a deviation about some mean function. The coefficients θ_μ are obtained by projecting this function into the span of the basis. The mean function used in the present analysis will be discussed in Section 5.1.

2.2 Optimization

The isentrope function $p(\rho)$ has degrees-of-freedom θ. The optimal model degrees of freedom are calibrated to a set of data, $\mathscr{Y}$ by solving an optimization problem with a Bayesian objective function, as in [1].

$$\theta^\star = \underset{\theta}{\text{argmax}} \left(\log \left(P(\theta | \mathscr{Y}) \right) \right). \quad (5)$$

Taking a Taylor series expansion of the log-posterior probability about an initial point, θ:

$$\log \left(P(\theta + \eta | \mathscr{Y}) \right) = \log \left(P(\theta | \mathscr{Y}) \right) + \eta \frac{\partial \log \left(P(\theta | \mathscr{Y}) \right)}{\partial \eta} \\ + \frac{\eta^2}{2} \frac{\partial^2 \log \left(P(\theta | \mathscr{Y}) \right)}{\partial \eta^2} + \mathscr{O}(\eta^3) m \quad (6)$$

and ignoring terms of $\mathscr{O}(\eta^3)$ and greater in the posterior, the optimization problem becomes:

$$\eta^\star = \underset{\eta}{\text{argmax}} \left(\log \left(P(\theta + \eta | \mathscr{Y}) \right) \right), \quad (7)$$

$$\theta^\star = \theta + \eta^\star. \quad (8)$$

The log-posterior probability is the sum of the log-prior probability and the log-likelihood. If both the prior and posterior are chosen to be Gaussian, then (6) is reduced to a quadratic function in η. This quadratic function has a simple analytic solution if η is unconstrained. Since the optimization coordinates given by (4) can admit physically implausible functions, some constraints must be applied to the problem.

The isentrope represents a function of pressure with respect to density. Since the HE products are a gas, they cannot be in tension so the function is constrained to be positive. The slope of the isentrope is equal to the square of the sound speed [25]. Since imaginary sound speeds are not physically meaningful, the slope must be positive. Finally, the isentrope must be convex in specific volume, (the reciprocal of density), unless there is a phase change occurring in the bulk material [16], which is not the case for HE detonation products. As an approximation to this final constraint, the isentrope is constrained to be convex in density.

Copyright © 2019 ASME

All these constraints can be expressed as linear inequality constraints in the basis $\Upsilon(\rho)$. Further details of how these constraints are formulated are given in [1].

The final optimization problem is:

$$\begin{aligned} \max \quad & P(\theta + \eta | \mathscr{Y}) \\ \text{with respect to} \quad & \eta \\ \text{such that} \quad & \mathbf{W}\eta \preceq \ell \end{aligned} \tag{9}$$

The solution to this constrained quadratic optimization problem give an optimal step $\eta^\star$ from the initial set of model degrees of freedom, θ, which maximizes the log-posterior probability of the model given the data, subject to the approximations inherent in (6). The true log-posterior probability, obtained from evaluating the log-prior probability and log-likelihood directly, is used to search along the line connecting θ to $\theta^\star$ in order to determine if a local minimum exists in the true probability distribution within these bounds. A naive parallel line search is used which divides this space into twelve equal steps and evaluates the posterior probability at each step. The point with the highest posterior probability is chosen as the starting point θ for the next step in this iterative optimization process. This process is described in more detail in [1].

3 Uncertainty Quantification

The Bayesian formulation of the objective function has several advantages when examining the uncertainty in the optimal model. Since the prior probability and likelihood are both Gaussian, the posterior covariance is well represented by the Laplace approximation, where the inverse of the posterior covariance is assumed to be equal to the Hessian of the log-posterior probability [1].

The expected value of the second derivative of the log-likelihood of an experiment with respect to the model degrees freedom is referred to as the Fisher information matrix. This quantity is easily calculated from the optimization results (See [1]). The Fisher information shows how each experiment contributed to the uncertainty in the final result. Since the basis $\Upsilon(\rho)$ is ortho-normal, the eigenvalues of the Fisher information matrix are the coefficients of eigenfunctions, *i. e.* a set of orthogonal functions showing the directions in function-space where the experiment constrains the result. Where the eigenfunctions are large in magnitude, the experiment is constraining, where they are small or zero, the experiment does not constrain the model. In this way, the influence of each experiment on the optimal solution can be better understood.

In the Laplace approximation, the inverse of the posterior covariance matrix is the sum of the Fisher information matrix for each experiment and the inverse of the prior covariance matrix. This posterior distribution, however, is not constrained to be feasible. Representing the function as a B-spline allows physically implausible functions to exist in the posterior distribution. To examine only feasible functions, random samples are drawn from the posterior and are accepted only if they are feasible with respect to the constraints applied in (9). This population of feasible samples can be projected into a direction of interest to get a univariate probability distribution which characterizes the uncertainty in the constrained posterior distribution in that direction.

This measure of uncertainty encompasses model-form uncertainty, parametric uncertainty and experimental uncertainty. The flexible B-spline basis can admit almost any feasible function to represent the model. Compared to a parametric model, almost all the uncertainty in the function is in the choice of B-spline coefficients, rather than the suitability of the functional form of the model. Additionally, since the uncertainty in the experimental data is reflected in the log-likelihood, the uncertainty bounds created by this method also include the experimental uncertainty. This procedure is applied to obtain the uncertainty in several quantities of interest in Section 5.5.

4 Experiments and Simulations

The optimization procedure requires data from multiple experiments to infer the EOS across a wide regime. Both a set of experimental data and a simulation which can use the EOS model to predict the experiment are needed. In several of the experiments, the thermodynamic properties of the EOS are not observed directly but are inferred from the observation of some more easily measured property of the experiment. In these cases, models are needed for the other physics processes involved in the experiment, which will have an influence on the optimal EOS model. However, these physics processes are much better understood than the EOS of HE detonation products and the model parameters are known with a greater degree of certainty. The EOS models obtained in this paper should have wider applicability to problems that involve different physics processes and materials. The three additional physics models were used in this analysis were: EOS for both HE reactants and copper, material strength for the copper, and HE burn. The details of these models and parameter choices are given in Appendix A.

4.1 Cylinder tests

A cylinder test is a standard experiment used to calibrate EOS models [7]. A one inch inner diameter copper cylinder[1] with a 0.1 inch thick wall is filled with one inch outer diameter pellets of high explosives. The cylinder is detonated at one end and after several diameters the detonation becomes a steady traveling wave. The radial motion of the cylinder wall is measured using Photon Doppler Velocimirty (PDV) probes, see Figure 1a. A set of experiments performed by Pemberton *et al.* [28]

---

[1]dead-soft C101

4

Copyright © 2019 ASME

(a) Cylinder test

(b) Sandwich test

(c) Gas gun [29]

(d) Explosively driven flyer plates
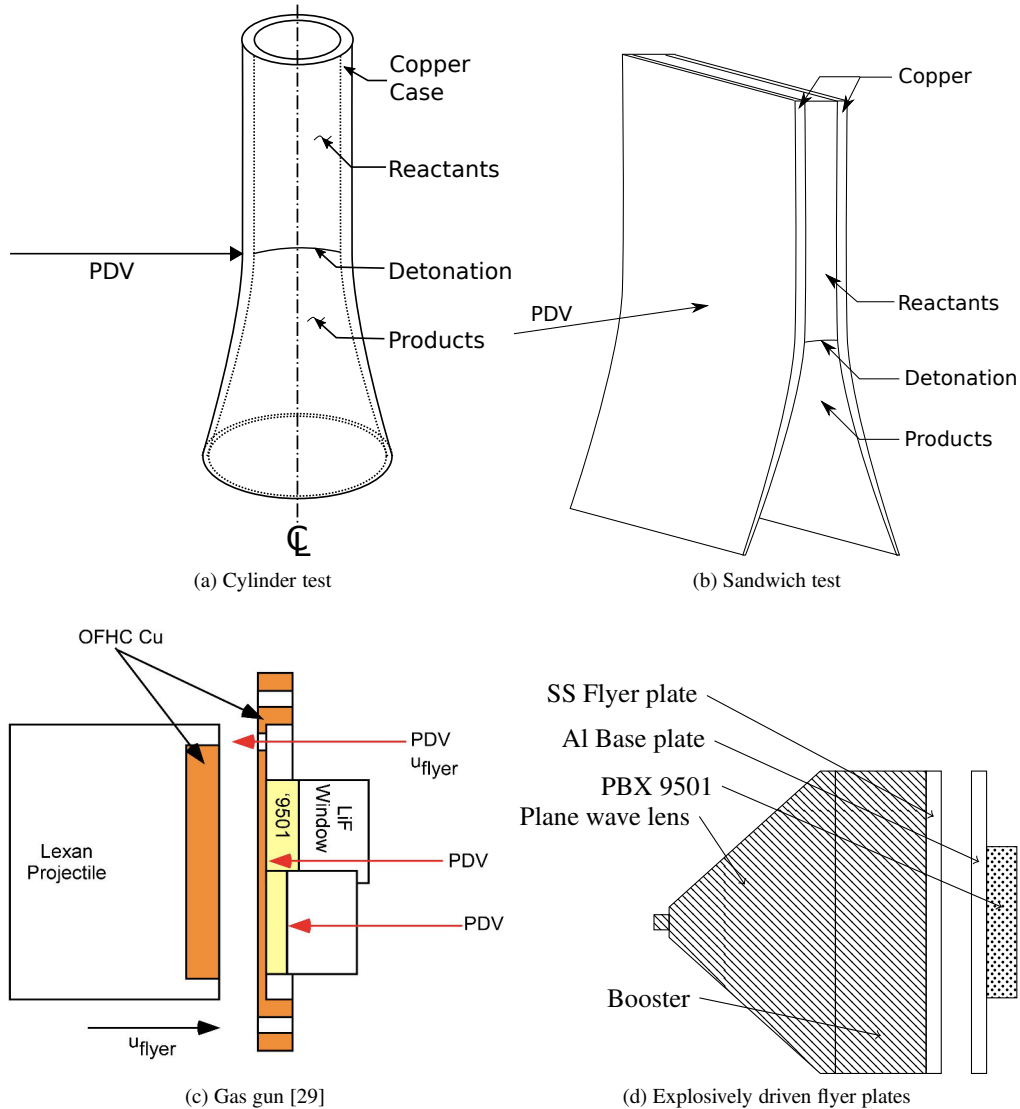
FIGURE 1: Different experiments used to examine equation of state

are used for model calibration. Five different cylinder tests were performed using nominally identical samples of HE. Two shots were were used as calibration data, the mean initial density of the HE reactants for both shots was $1.835\,\mathrm{g\,cm^{-3}}$. Each test was instrumented with two linear arrays of PDV probes, aligned with the long axis of the cylinder and installed at two different angles. The PDV probes recorded the velocity history of the outer surface of the cylinder. The axial location of the first probe was placed far enough from the detonator that the detonation wave was believed to have obtained a steady traveling profile. It was non-trivial to account for the uncertainty in the PDV measurements given notable shot-to-shot and probe-to-probe variations in measurements of what were nominally identical conditions.

Appendix B describes the procedure which was developed to obtain an estimate of the covariance matrix for one of the cylinder velocity histories.

The detonation wave proceeded along the cylinder at near the CJ state. Downstream of the detonation wave the expanding products of detonation drove the cylinder wall outwards, leading to pressures below the CJ state. Therefore, the cylinder experiments only examined states less than CJ and provided no information at pressures above this state.

4.1.1 Simulation The cylinder test was simulated in the Lagrangian hydrodynamic simulation code FLAG [6]. The experiment was modeled in two-dimensional axi-symmetric co-

Copyright © 2019 ASME

ordinates. Three other physics models were used in the simulation. The solid EOS for the copper was modeled using linear a U_s-U_p EOS model, as described in Appendix A.1. The material strength of the copper was modeled using the PTW model [30] for the deviatoric stress in the solid, as described in Appendix A.2. Additionally, the propagation of the detonation along the cylinder was modeled using a 'programmed burn' method, using Detonation Shock Dynamics (DSD) to compute the lighting times for the HE, as described in Appendix A.3.

4.2 Explosively driven flyer plates

The explosively driven flyer plate experiments conducted by Fritz *et al.* [14] used an explosive lens to accelerate a plate of stainless steel into a 6061 aluminum base-plate on which the HE samples were mounted, see Figure 1d. The initial density of the HE samples for all experiments was $1.836 \pm 0.002\,\mathrm{g\,cm^{-3}}$. The time history of the light emitted from the interface of the HE samples and a thin layer of a noble gas allowed measurements of both the shock speed and particle speed in the HE detonation products and the sound speed in these gases. The experimental data were given as pairs of shock speed U_s and associated particle speed U_p on the Hugoniot. Sound speed data on the Hugoniot were also given for a range of detonation product densities.

The explosively driven flyer plates induced pressures much greater than the CJ pressure in the HE and these experiments examined overdriven states of the EOS.

4.2.1 Simulation
The equation of state model could be used directly to evaluate the data obtained by Fritz *et al.* without using expensive numerical simulations. The thermodynamic relationships given by Fickett and Davis [12] provided the shock speed and particle speed on the Hugoniot. Similarly, the EOS model could be manipulated to yield sound speed on the Hugoniot analytically (see [11]).

4.3 Gas-gun experiments

4.3.1 Experiment
Similar to the explosively driven flyer plates, gas-gun tests [29] used compressed air rather than high explosives to accelerate a copper impactor into a copper base plate on which the HE samples were mounted, see Figure 1c. A Lithium Fluoride (LiF) window was mounted to the back the the HE sample and a PDV probe measured the velocity of the HE LiF interface. The experimental data are provided as time histories of this interface. After the initial shock from the accelerated plate reached the interface, the velocity reached a plateau for a few tenths of a microsecond. This velocity plateau can be determined through an impedance match between the HE EOS and the EOS for the two solids, copper and LiF.

The gas gun induced pressures greater than the CJ state in the HE detonation products so this experiment also gave infor-

TABLE 1: Flyer plate velocities for gas gun shots [29]

Shot ID	Velocity / $\mathrm{cm\,\mu s^{-1}}$	Initial HE density / $\mathrm{g\,cm^{-3}}$
2S-799	0.3032	1.834 ± 0.003
2S-800	0.3316	1.835 ± 0.003
2S-812	0.3184	1.835 ± 0.003
2S-832	0.3466	1.834 ± 0.003

mation at densities and pressures greater than CJ. Since only the velocity plateau in the time history was analyzed, each shot only gives information about a small range of densities. Four different shots were considered, each shot fired was fired with a different velocity for the flyer plate, shown in Table 1.

4.3.2 Simulation
The approach described in Cooper [8] is used to calculate the interface velocity between the HE detonation products and the LiF window. It is a assumed that the solid PBX 9501 used in the experiment is instantaneously converted into gaseous products on contact with the flyer. This assumption is reasonable given the small reaction zone size of this HE formulation. First, the compatible state between the moving flyer and the stationary HE products is obtained. The pressure, internal energy and velocity of the gasses in this state are used to find the compatible state between the shocked HE products and the stationary LiF window.

The impedance matching procedure requires an EOS for both the HE and the solids. A linear U_s-U_p EOS model was used to model both copper and lithium fluoride. The constants used in this model are given in Appendix A.1

4.4 Sandwich tests

The sandwich test is an experiment which is very similar to a cylinder test but uses planar rather than cylindrical geometry [19, 34]. The experiment was conducted using a PBX 9501 charge that was 130 mm along the direction of detonation propagation, and 150 mm in the direction normal to propagation. The density of the charge was 1.8327 g cm^{-3}, measured by water immersion. The thickness of the charge was 10.03 mm, measured at 10 evenly spaced locations along the centerline, each PDV probe measurement location, and each of the corners. Angstrom Bond AB9320 was used to bond copper plates to the PBX 9501 charge. The thickness of the annealed, C101 copper confining plates and the final thickness of the assembly were measured at the same locations so that the thickness of the glue layer could be inferred. The plates were each found to be 1.02 mm thick and the final assembly thickness was 12.11-12.12 mm, indicating a glue layer thickness of approximately 0.020-0.035 mm on each side.

Four PDV probes were used to measure confiner velocity profiles at 2/3 of the run distance. In the direction normal to detonation propagation, the probe position varied, with two located at the centerline (one probe on each side of the assembly), one 10 mm offset from centerline, and the final probe 20 mm offset from centerline. The velocity profile from a single probe located on the centerline of the experiment was used as validation data for the model.

4.4.1 Simulation The sandwich test was modeled in a similar manner to the cylinder test, except it used Cartesian rather than axi-symmetric coordinates. The simulation used the same additional physics models as the cylinder experiment.

5 Optimization results
5.1 Problem definition
The EOS model spanned a regime in density of $0.1\,\mathrm{g\,cm^{-3}}$ to $4\,\mathrm{g\,cm^{-3}}$. The B-spline basis consisted of 75 knots equi-log spaced across the range in densities. The fractional uncertainty in the pressure function for the prior was $\alpha_m = 3.24\%$ and the characteristic correlation distance was $\sigma_m = 2.4$ times the distance between the knots in log-density. These choices of how to construct the B-spline basis and the kernel used to create the optimization basis $\Upsilon(\rho)$ were based on the results of a previous study, [1], which found that these choices allowed the flexibility to represent a large space of possible functions while allowing a sufficiently large fraction of feasible samples to be drawn from the posterior distribution.

The mean function was chosen to be a power law,

$$p(\rho) = 2.56\,\mathrm{GPa\,cm^9\,g^{-3}}\rho^3. \tag{10}$$

This functional form is the simplest EOS model described by [21]. The two coefficients in the model, the leading constant and the power, were chosen to be similar those used for the HE formulations in [21]. The prior function is intentionally chosen to be a coarse approximation to show the ability of the algorithm to improve the model so it is in agreement with multiple experiments.

There were four different kinds of experiments in the set of all data, $\mathscr{Y}$.

1. Pemberton *et al.* cylinder tests [28]. Shot 1 and 2 probes 1 - 7
2. Fritz *et al.* overdriven Hugoniot data. All points from Table 1 in [14]
3. Fritz *et al.* overdriven sound speed measurements. All points from Table 3 in [14]
4. Pittman *et al.* [29] gas gun experiments. Shots 2S-799, 2S-800, 2S-8112 and 2S-813
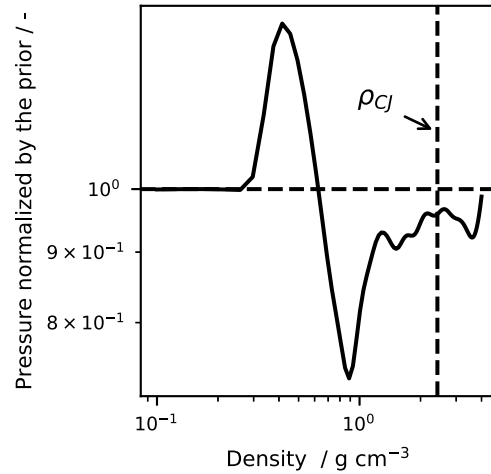
FIGURE 2: Deviation of the optimal equation of state model obtained from the optimization procedure from the prior. The vertical axis is the pressure on the optimal isentrope divided by the pressure on the prior model for the isentrope

5.2 Results
The optimization was performed using twenty nodes of the LANL HPC cluster 'snow'. Each node consisted of two 18 core 2.1 GHz Intel Xenon Broadwell processors for a total of 720 processors. Three iterations of the optimization procedure were required for the problem to converge, taking approximately 36 hours.

The optimal model is shown in Figure 2. The model is unchanged at low densities but at higher densities the optimal model differed from the prior. The effects of the prior and the optimal model on the simulations is shown in Figure 3. In all four experiments, the prior model did a poor job at predicting the experimental data. The optimal model brought the simulations into good agreement with the experimental data. More insight into which regime in density was influenced by each experiment can be obtained by examining the Fisher information for each experiment.

5.3 Fisher information
The influence of each experiment on the optimal solution can be better understood by considering the Fisher information for each experiment. The eigenfunctions of the Fisher information matrix corresponding to large eigenvalues show where the experiment was most constraining. Figure 4b shows that the cylinder experiment was very influential near the CJ state and continued to provide some information at lower densities. Figure 4d shows the eigenfunctions of the Fisher information for

(a) Cylinder Shot 1 PDV 1

(b) Gas Gun Shot 2S832

(c) Overdriven Hugoniot

(d) Overdriven Sound Speed
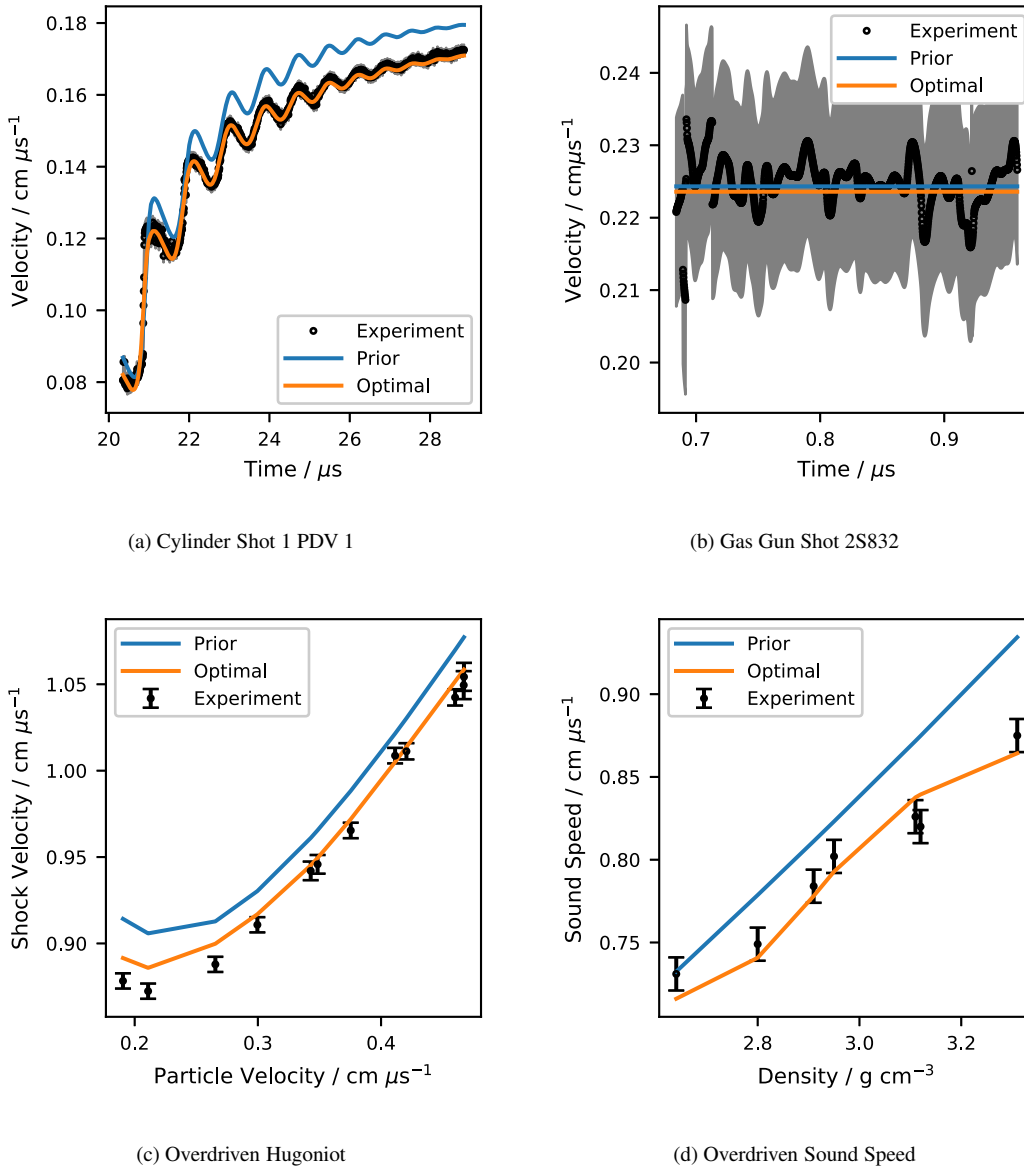
FIGURE 3: Comparison of four characteristic simulations using the prior and optimal isentrope models

a gas-gun shot, this experiment provided information at over-driven densities but provided very little information at densities below CJ. Since only the overdriven state was examined in the gas-gun shots, this result is expected. Examining the Fisher information can help show why a certain optimal function was obtained and can also guide the design of future experiments by understanding how each experiment constrained on the result.

5.4 Validation

The predictive ability of the EOS model was examined by simulating a sandwich experiment, which was not included in the data used for model calibration. The simulation using the optimal EOS, Figure 5, showed good agreement with the experiments. The poor agreement in the early cycles of the ringing was likely due to the temporal resolution of the PDV probes. The velocity history also slightly under-predicted the velocity of the copper plates at late times.

(a) Cylinder Shot 1 PDV 1 eigenvalues

(b) Cylinder Shot 1 PDV 1 eigenfunction

(c) Gas Gun Shot 2S832 eigenvalues

(d) Gas Gun Shot 2S832 eigenfunction

FIGURE 4: Comparison of the eigenvalues and eigenfunctions from two different experiments.

5.5 Uncertainty quantification

The uncertainty quantification methods described in Section 3 converted the multivariate probability distribution for the model degrees of freedom into a univariate distribution by projecting feasible samples in a specified direction. This univariate distribution could be used to obtain samples which represented the $\pm95\%$ confidence interval of the distribution in that direction. The choice of direction had a significant effect on the uncertainty bounds given by this method. Several directions were considered, including the directions which diagonalized the posterior covariance matrix. The set of directions, however, which gave the most realistic confidence intervals was the direction of greatest sensitivity to each Quantity Of Interest (QOI). These directions were obtained using a finite difference approach and each direction was specific to a given QOI. Two QOI's for the EOS model are shown in the first two rows of Table 2, the uncertainty bounds on these two quantities bracket experimentally measured values not used directly in the calibration. A more complicated quantity of interest involved the ability of the sandwich experiment to do work on the confining material. The quantity of in-

9

FIGURE 5: Time history of PDV probe from a sandwich test [19, 34], compared to a FLAG simulation performed using the optimal HE EOS model

terest for this experiment was the velocity of the metal casing after it had been displaced outwards by 4 mm. The cumulative distribution of the feasible samples in the direction of greatest sensitivity for this QOI is shown in Figure 6a. Simulations run with three samples from this CDF representing the mean, upper and lower 95% confidence interval are shown Figure 6b. Though the differences between the three simulated velocity histories is almost imperceptible in this Figure, they led to a 0.4% difference in the QOI, shown in the last row of Table 2.

6 Conclusion

The procedure described in this paper identified an equation of state model for the detonation products of high explosives which was a best fit to multiple experiments which probed a wide range of densities at states both above and below the CJ point. The semi-parametric model formulation allowed a wide range of possible functional forms to be examined and the Bayesian formulation of the optimization used for model calibration provided some insight into the uncertainty in the model and its predictive capability.

The model was validated, and showed good agreement with an experiment outside the set of calibration data. Uncertainty bounds on several predicted quantities of interest were calculated. The relative magnitude of the uncertainty depended on the quantity of interest, so the predictive ability of the model must be assessed with respect the the application of interest.

REFERENCES

[1] Stephen A. Andrews and Andrew M. Fraser. Estimating physics models and quantifying their uncertainty using optimization with a bayesian objective functional. *ASME Journal of Verification Validation and Uncertainty Quantification*, 2019. In review.

[2] Tariq D. Aslam. Detonation shock dynamics calibration of PBX 9501. In M. Elert, M. D. Furnish, R. Chau, N. Holmes, and J. Nguyen, editors, *Shock Compression of Condensed Matter*, volume CP955, pages 813–816, 2007.

[3] Tariq D. Aslam. Shock temperature dependent rate law for plastic bonded explosives. *Journal of Applied Physics*, 123(14):145901, 2018.

[4] Tariq D. Aslam and Mark Short. Detonation shock dynamics overview and calibration. LA-UR 1326358, Los Alamos National Laboratory, 2013. Sponsor: DOE/LANL.

[5] Tariq Dennis Aslam. PRZ calibration for PBX 9501 (PBX9501/L2-2015). LA-UR 15-27328, Los Alamos National Laboratory, 2015.

[6] Donald E. Burton. Connectivity structures and differencing techniques for staggered-grid free-lagrange hydrodynamics. UCRL JC-110555, Lawrence Livermore National Laboratory, Livermore, CA, 1992.

[7] Richard Catanach, Larry Hill, Herbert Harry, Ernest Aragon, and Don Murk. Cylinder test specification. LA 13643-MS, Los Alamos National Laboratory, Los Alamos, NM, 1999.

[8] Paul W. Cooper. *Explosives engineering*. Wiley, 1996.

[9] P. Dierckx. *Curve and surface fitting with splines*. Monographs on Numerical Analysis. Oxford University Press, 1993.

[10] B. M. Dobratz and P. C. Crawford. LLNL explosives handbook. Technical Report LLNL-UCRL-5997-Chg.2, Lawrence Livermore National Laboratory, Livermore, CA, 1985.

Copyright © 2019 ASME

(a) Projection of the feasible posterior samples in the direction of greatest sensitivity to the sandwich test QOI

(b) Sandwich test simulations performed at the $\pm 95\%$ confidence interval on the QOI

FIGURE 6: Uncertainty quantification

TABLE 2: Uncertainty bounds on properties of the EOS model and simulation predictions

QOI		Lower 95%	Mean	Upper 95%	Experiment
CJ Pressure	Mbar	0.347	0.350	0.358	0.348 [14]
CJ Detonation Speed	$\mathrm{cm\,\mu s^{-1}}$	0.883	0.886	0.888	0.883 [10]
Sandwich wall velocity at 6 mm	$\mathrm{cm\,\mu s^{-1}}$	0.2237	0.2240	0.2246	0.2242

[11] Ronald P Fedkiw, Tariq Aslam, Barry Merriman, and Stanley Osher. A non-oscillatory eulerian approach to interfaces in multimaterial flows (the ghost fluid method). *Journal of Computational Physics*, 152(2):457 – 492, 1999.

[12] Wildon Fickett and William C. Davis. *Detonation: theory and experiment*. Dover, Mineola, NY, 2000.

[13] David A. Fredenburg, Tariq Dennis Aslam, and Langdon Stanford Bennett. A Gruneisen equation of state for TPX: application in FLAG. LA-UR 15-28533, Los Alamos National Laboratory, 2015.

[14] J. N. Fritz, R. S. Hixson, M. S. Shaw, C. E. Morris, and R. G. McQueen. Overdriven-detonation and sound-speed measurements in PBX-9501 and the "thermodynamic" Chapman–Jouguet pressure. *Journal of Applied Physics*, 80(11):6129–6141, 1996.

[15] R. S. Hixson, M. S. Shaw, J. N. Fritz, J. E. Vorthman, and W. W. Anderson. Release isentropes of overdriven plastic-bonded explosive PBX-9501. *Journal of Applied Physics*,

88(11):6287–6293, 2000.

[16] Yasuyuki Horie, editor. *Solids I*, volume 2 of *ShockWave Science and Technology Reference Library*. Springer Berlin Heidelberg, 2007.

[17] John D. Hunter. Matplotlib: a 2D graphics environment. *Computing in Science & Engineering*, 9:21–29, 2007.

[18] Frank P. Incropera and David P. DeWitt. *Fundamentals of Heat and Mass Transfer*. Wiley, fifth edition, 2002.

[19] Scott Jackson, Eric Anderson, Tariq Aslam, and Von Whitley. Comparison of slab and cylinder expansion test geometries for PBX 9501. In *Proceedings of the 20th Biennial Conference of the APS Topical Group on Shock Compression of Condensed Matter*, St. Louis, MI, July 2017.

[20] Eric Jones, Travis Oliphant, Pearu Peterson, et al. SciPy: open source scientific tools for Python, 2001–2018. [Online; accessed 07-06-18].

[21] E. L. Lee, H. C. Hornig, and J. W. Kury. Adiabatic expansion of high explosive detonation products. techreport

UCRL-50422, Lawrence Radiation Laboratory, Livermore CA, 1968.

[22] Stanford P. Lyon and James D. Johnson. SESAME: the Los Alamos National Laboratory equation of state database. LA-UR 92-3407, Los Alamos National Laboratory, 1992. Classification (full-text): U.

[23] P. Marsh, Stanley. *LASL Shock Hugoniot Data.* University of California Press, 1980.

[24] Ralph Menikoff. Deflagration Wave Profiles. LA-UR 12-20353, Los Alamos National Laboratory, 2012.

[25] Michael J. Moran and Howard N. Shapiro. *Fundamentals of engineering thermodynamics.* John Wiley & Sons, 5th edition, 2004.

[26] William L. Oberkampf and Christopher J. Roy. *Verification and Validation in Scientific Computing.* Cambridge University Press, Cambridge, UK, 2012.

[27] T. Oliphant. *A guide to NumPy.* Trelgol Publishing, 2006.

[28] Steve J Pemberton, Tom D Sandoval, Tommy J Herrera, John A Echave, and Garry Maskaly. Test report for equation of state measurements of PBX-9501. LA-UR 11-04999, Los Alamos National Laboratory, Los Alamos, NM, 2011.

[29] Emily R. Pittman, Carl R. Hagelberg, Richard L. Gustavsen, and Tariq D. Aslam. Gas gun experiments and numerical simulations on the HMX based explosive PBX 9501 in the overdriven regime. *AIP Conference Proceedings*, 1979(1):150032, 2018.

[30] D. L. Preston, Davis L. Tonks, and Duane C. Wallace. Model of plastic deformation for extreme loading conditions. *Journal of Applied Physics*, 93(1):211–220, 2003.

[31] Carl Edward Ramussen and Christopher K. I. Williams. *Gaussian processes for machine learning.* Adaptive Computation and Machine Learning. The MIT Press, Cambridge, MA, 2006.

[32] P. A. Rigg, M. D. Knudson, R. J. Scharff, and R. S. Hixson. Determining the refractive index of shocked [100] lithium fluoride to the limit of transmissibility. *Journal of Applied Physics*, 116(3):033515, 2014.

[33] JL Wise and LC Chhabildas. Laser interferometer measurements of refractive index in shock-compressed materials. In Y. M. Gupta, editor, *Shock waves in condensed matter*, pages 441–454. Springer, 1986.

[34] Marvin A. Zocher, Tariq D. Aslam, Scott I. Jackson, and Eric K. Anderson. Numerical modeling comparing slab to cylinder test expansion geometries for PBX 9501. In *Proceedings of the 16th international detonation symposium*, Cambridge MD, 2018.

[35] Marvin A. Zocher, Paul J. Maudlin, Shuhrong Chen, and Elane C. Flower-Maudlin. An evaluation of several hardening models using taylor cylinder impact data. LA-UR 00-1192, Los Alamos National Laboratory, Los Alamos, NM, 2000.

A Other physics models
A.1 Solid equation of state

The solid equation of state was modelled as a Mie Grüeneisen form using a reference curve derived from a linear relationship between U_s and U_p. The formulation of such an EOS is described in [8] and [13]. Sets of coefficients for this model for various solids are given in Table 3.

A.2 Material strength

The material strength of highly deformed metals was modeled using the PTW formula for flow stress as a function of strain rate and temperature [30]. Model coefficients for copper are given in [30]. Additionally, a model is needed for how the melt temperature and cold shear modulus vary with density. These effects are modeled by interpolation onto SESAME tables [22].

A.3 Detonation Shock Dynamics (DSD)

The FLAG simulations could not directly model the propagation of a detonation wave through the HE. The detonation wave was modelled using a DSD approach [4] when the arrival time of the detonation wave throughout the computational domain was pre-computed. The DSD approach must be calibrated to the specific HE formulation of interest. These calibration parameters for PBX 9501 are given in [2].

B Uncertainty in Cylinder tests

There were known non-uniformities in the thickness of the cylinder wall in the data from Pemberton *et al.* [28]. A model for the correlated errors in the cylinder test data was needed to accurately represent the uncertainty in the experimental data.

There were n_{shot} time histories, $y_i(t_i)$. Each time history was sampled using different non-uniform time-steps. The data are modeled as a mean function plus a zero-mean deviation function and IID noise.

$$y_i(t_i) = \mu(t_i) + \delta(t_i) + \varepsilon \tag{11}$$

Project each time history into a basis of n_{basis} cubic B-spline functions. The number of basis functions is chosen *a priori* to minimize the MSE error between a single time history and its representation is the basis.

$$c_i = \langle B(t_i), B(t_i) \rangle^{-1} \langle B(t_i), y_i \rangle \tag{12}$$

Calculate the mean squared error between the spline function and the data

$$MSE_i = \frac{1}{n_t} \sum (y_i(t_i) - B(t_i)c_i)^2 \tag{13}$$

TABLE 3: Linear U_s - U_p coefficients for solids

Material	C (cm μs^{-1})	s	C_v (100MJ/kg)	ρ_o (g cm^{-3})	Γ
Copper	0.397 [32]	1.479 [32]	0.385×10^{-5} [18]	8.93 [32]	2.02 [35]
Lithium fluoride	0.5148 [33]	1.353 [33]		2.640 [33]	0.0
PBX9501 reactants	0.290 [23]	1.44 [23]	10.88×10^{-6} [5]	1.835	0.0

Since B-splines are linear in their coefficients, the mean of the basis function coefficients is the mean function.

$$\bar{c} = \frac{1}{n_{shot}} \sum_{i=1}^{n_{shot}} c_i \qquad (14)$$

$$\mu(t) = B(t)\bar{c} \qquad (15)$$

The mean function by definition has no covariance. The deviation function has zero-mean. The covariance of the deviation function is:

$$\mathbb{E}\left(\delta(t)^2\right) = k_\delta = \text{cov}(c - \bar{c}), \qquad (16)$$

and the IID noise is,

$$\mathbb{E}\left(\varepsilon^2\right) = \frac{1}{n_{shot}} \sum_{i=1}^{n_{shot}} MSE_i. \qquad (17)$$

Thus the covariance matrix for a specific shot is:

$$\mathbb{E}\left(y_i(t_i) - \mu(t_i)\right) = B(t_i)k_\delta B(t_i)^T + \mathbb{E}\left(\varepsilon^2\right)\mathbb{I} \qquad (18)$$